Nano-alignment in semiconducting polymer films: A path to achieve high current density and brightness in organic light emitting transistors

Mujeeb Ullah Chaudhry,*[,1] Khalid Muhieddine,[1] Robert Wawrzinek,[1] Jun Li,[2] Shih-Chun Lo,*[,3]

Ebinazar B. Namdas*[,1]

[1] Centre for Organic Photonics & Electronics, School of Mathematics and Physics, The University of Queensland, Brisbane, QLD 4072, Australia.

[2] Institute of Materials Research and Engineering (IMRE), Research Link, Singapore.

[3] Centre for Organic Photonics & Electronics, School of Chemistry and Molecular Biosciences, The University of Queensland, Brisbane, QLD 4072, Australia.

*Correspondence to: mujeeb.ullah@uq.edu.au, s.lo@uq.edu.au, e.namdas@uq.edu.au

Abstract:

Organic light emitting field effect transistors (LEFETs) integrate light-emission of a diode with logic functions of a transistor into a single device architecture. This integration has the potential to provide simplified displays at low costs and access to injection lasing. However, the charge carrier mobility in LEFETs is a limiting factor in realising high current densities along with a trade-off between brightness and efficiency. Herein, we present a technique controlling the nanoscale morphology of semiconducting polymers using nanoscale grooved substrates and dip coating deposition to achieve high current density. We then applied this approach to heterostructure LEFETs and demonstrated brightness exceeding 29,000 cd m^{-2} at an EQE of 0.4% for a yellow emitter and 9,600 cd m^{-2} at EQE of 0.7% for a blue emitter. These results represent a significant advancement in organic optoelectronics and are an important milestone towards realisation of new applications in displays and electrically pumped lasing.

1. Introduction

Organic light emitting field effect transistors (LEFETs) have been attracting significant attention as they integrate light-emission of an organic light emitting diode (OLED) with logic functions of an organic field effect transistor (OFET) in one single device.[1–8] This integration provides access to low cost and simplified display pixels as it removes the requirement of separate high mobility-driving transistors.[4,9,10] An LEFET structure also has the potential to be applied in electrically pumped lasing due to low optical losses (generally associated with detached electrodes) and the capability to achieve high current densities - hence a high brightness required by the lasing threshold.[11–16] Over the past decade, significant progress has been made to simultaneously improve the external quantum efficiency (EQE), current density, brightness and mobility of LEFETs.[17–19] Despite tremendous progress, to date the mobility and brightness achieved in polymer based LEFETs remain low.

To advance this field towards electrically pumped lasing, two major obstacles have to be overcome: i) realisation of high current density/mobility, low optical losses and development of robust charge transporting semiconducting materials, and ii) achieving high brightness combined with high EQE. For more than a decade significant efforts have been directed towards the quest for high mobility charge transporting semiconducting polymers. However, π-conjugated polymers tend to form disordered structures due to a high degree of conformational freedom. This disorder potentially impedes the charge transport and reduces the mobility. One effective way to reduce disorder is to align the semiconducting polymer chains. This can be achieved via directional solidification and thermal/solvent annealing during the film formation process.[19–23] Recently, Heeger *et al.*, achieved OFET hole mobilities as high as 47 $cm^2\ V^{-1}\ s^{-1}$ in macroscopically aligned semiconducting polymers.[21] Similar polymers in LEFETs were also reported by the same group, albeit with a low current density and mobility (0.5 $cm^2\ V^{-1}\ s^{-1}$).[19]

Here, we show a simple and powerful strategy to align a semiconducting polymer and demonstrate its effectiveness in bilayer LEFETs with a record-breaking brightness exceeding 29,000 cd m^{-2} at an EQE of 0.4% for a yellow emitter and 9,600 cd m^{-2} at EQE of 0.7% for a blue emitter. These devices outperform the best LEFETs reported in literature to date. The LEFETs comprise of a highly aligned hole transporting diketopyrrolopyrrole based copolymer (DPP-DTT)[24] in conjunction with a light-emitting polymer, Super Yellow (SY), or a light emitting small molecule, 9-(9-phenylcarbazole-3-yl)-10-(naphthalene-1-yl)anthracene (PCAN). We align DPP-DTT into highly oriented chains using nano-grooved substrates and

solvent dip coating. A large anisotropy in the mobility values along the parallel and perpendicular direction of the DPP-DTT polymer chain was observed - along the DPP-DTT polymer chains, the mobility is significantly higher than perpendicular to the grooves.

2. Device Fabrication

The uniaxial nano-grooves on a substrate were fabricated by scratching the 600 nm thick $SiNx/SiO_2$ dielectric surface using a diamond lapping film with nanoparticle diameters of 100 nm.[20,21,23] The grooved substrates were then thoroughly cleaned (see methods section) and treated with decyltrichlorosilane (DTS). A solution of DPP-DTT (M_w = 349,000 g mol^{-1}, PDI = 2.8) in chloroform (99.9%, anhydrous) with a concentration of 1 mg mL^{-1} was prepared, sealed in a pressure tube, stirred on a hotplate (120 °C) for 2 hours and then kept at room temperature for at least 7 days to completely dissolve the polymer. The grooved substrates were vertically submerged into the hot polymer solution for 20 s and then gently removed at a rate of 0.2 mm s^{-1} to form a wet film. The coating procedure was performed under ambient atmosphere (air) to allow for slow evaporation of the solvent at the substrate's surface, providing enough time for the individual polymer chains to reorganise and orient themselves along the grove direction. It is important to note that prior to the dip-coating procedure, complete solubilising of individual polymer chains in the solvent is essential to achieve the best results. Full details of the fabrication and testing protocols and chemical structures of materials are presented in the methods section and **Figures S2** and **S3.**

3. Results and Discussion

3.1 Morphology

Figures 1a and **1b** show high-resolution atomic force microscopy (AFM) images of the scratched and control (unscratched) substrates. The scratched substrates exhibited an array of grooves of several microns in length, ≈5 nm in depth and ≈100 nm in width. For the control substrates, we observed a root-mean-square (RMS) surface roughness of ≈0.2 nm. **Figures 1c** and **1d** show the topography of DPP-DTT films on the scratched and control substrates, respectively. On the former, well-aligned and highly dense formation of nanofibers is observed; whereas on the control substrate, the topography is generally disordered and with clusters of nanofibers in some areas. To further probe the film morphology, we performed X-ray diffraction (XRD) on the polymer on scratched and control substrates. The polymer film on the

control substrate did not show any diffraction peaks, indicating a strong disorder, which is in good agreement with the AFM images (see **Figures 1e** and **1f**). For the scratched sample, the DPP-DTT film showed a strong diffraction peak at $2\theta \approx 4°$, corresponding to an interlayer spacing of ≈21.7 Å. This is close to the alkyl side-chain packing (100) of the crystalline lamellae formed via intermolecular end-to-end interactions. A π-π stacking diffraction peak was not observed with our experimental set-up.

3.2 Current Voltage Characteristics

Figure 2 shows the device structure and electrical characteristics of OFETs. Under p-type voltage bias, the devices demonstrate linear and saturation regimes with current ON/OFF ratios of $>10^5$. On a flat surface, we found an isotropic drain current in contrast to the highly anisotropic behaviour on the grooved substrates. The drain current along parallel to the grove is at least >10 times higher than in perpendicular direction (see **Figure 2**). This can be explained by a parallel long-range alignment of the DPP-DTT polymer chains along the nano-grooves. Such configuration governs charge transport due to charge delocalisation along the π-conjugated polymer backbone. Here the charges move freely along the polymer backbone with just occasional 'hopping' between adjacent polymer chains on their journey through the transistor channel.[20,21,23] In contrast, charges travelling perpendicular to the polymer backbone have to hop more frequently between adjacent polymer chains resulting in a reduced drain current.

3.3 Mobility Extraction

The saturation charge carrier mobility (μ) and threshold voltage (V_{TH}) were calculated from the transfer characteristics of the devices in the saturation regime using

$$I_{DS} = \frac{W C_i}{2 L} \mu (V_{GS} - V_{TH})^2 \quad (1)$$

where I_{DS} is the measured source drain current, V_{GS} the corresponding gate voltage, W/L the width-to-length ratio of the device channel and C_i the capacitance of the SiO_2/SiN_x dielectric. The measured gate capacitances were 5.2 and 5.6 nF cm^{-2} for flat and nano-grooved substrates, respectively (see **Figure S4**, Supplementary Information).

Next, we focussed on mobility extraction for control and nano-grooved substrates. We observed "two slopes" in plot of SQRT(I_{DS}) *versus* V_{GS} (see **Figure 3**) for all devices. The slopes of fitting SQRT(I_{DS}) *versus* V_{GS} data provide the high and low mobility values when evaluated from equation 1. The nano-grooved devices yield mobilities of 11±3 cm^2 V^{-1} s^{-1} at

V_{GS} = 0 to -70V; and 5±2 $cm^2\ V^{-1}\ s^{-1}$ at V_{GS} > -70 V. We have analysed data from at least 50 samples and found "two slopes" at low and high gate voltage regions, leading to an average mobilities of 5 $cm^2\ V^{-1}\ s^{-1}$ and 13 $cm^2\ V^{-1}\ s^{-1}$ at low and high gate voltages, respectively. Similarly, a two slopes behaviour was also observed in samples with flat surfaces obtaining a mobility of 0.8±0.4 $cm^2\ V^{-1}\ s^{-1}$ at lower V_{GS} and a mobility of 2±1 $cm^2\ V^{-1}\ s^{-1}$ at higher V_{GS}.

The origin of double slopes will be discussed in next section. Double slopes invalidate the MOSFET equation and lead to overestimation of mobilities. This can set an erroneous benchmark for device design. To assess critically the extracted mobility in our transistors, we calculated the "reliability factor", *r*, and effective mobility ($\mu_{eff} = r\ \mu$) of our devices as suggested by Podzorov *et al.*[25] The reliability factor r simply equals to the squared ratio of the slope of an electrically equivalent FET to the slope actually used to calculate the claimed mobility (μ). The reliability factor in both aligned and control samples were calculated for lower and higher slopes (see **SI** for details). The results are summarized in **Table 1.** The aligned sample exhibit an effective mobility of 9.4 $cm^2\ V^{-1}\ s^{-1}$, which is significantly higher than the effective mobility of control samples on a flat substrate (1.6 $cm^2\ V^{-1}\ s^{-1}$). These results confirm, swift charge transport along the π-conjugated polymer backbone.

3.4 Origin of Two Slopes

Now we focus on the origin of two slopes behaviour in our transistors. A large number of organic semiconductors materials including single-crystals[26] aligned polymers,[21,23] high mobility polymers[24] and small molecules[22,27] have shown "two slopes" in transistor transfer characteristics. However, it is interesting to note that there is a paucity of information in the literature on the origin of such behaviour. To address this issue, we considered two potential factors that may contribute to the gate voltage dependent mobility. The first is electron injection from the opposite electrode, and the second contact resistance at source/drain electrodes. As DPP-DTT is a low band gap polymer with high electron affinity (≈3.5 eV), electron injections at high source-drain field (V_{DS} = -100 V) and low gate voltages for short channel devices cannot be ruled out. Under this circumstance, localised electron traps near one of the electrode invalidate the use of MOSFET equation derived from the gradual channel approximation. Moreover, contact resistance often shows dependency of gate voltage and results in complex and nonlinear electrical properties. To further understand the effect of contact resistance on device performance, we employed a four-point probe experimental setup to extract more accurate mobilities.

Figure 3b inset shows the gate four-point probe (gFPP) geometry. Sense probes at voltages (V1, V2) corresponding to the channel voltage at the probe positions. The gFPP method enables the evaluation of intrinsic mobility (*i.e.*, free from contact resistance) at variable gate voltages. It assumes a linear potential drop along the channel, which holds true at low source drain voltage. The conductivity σ is a sheet conductance determined by four-probe measurements and given as:

$$\sigma = \left(\frac{I_{\mathrm{DS}}}{|V_1 - V_2|}\right) \left(\frac{L_{\mathrm{probe}}}{W}\right) \quad (2)$$

where V_1 and V_2 are the measured probe potentials in the middle of the channel region, and L_{probe} is the distance between the probes (100 μm). The optical image of the devices is given in inset of **Figure 3**, where L_{probe} was 100 μm and channel length L was 500 μm and channel width W of the channel was 1000 μm. The gFPP mobility was calculated using the following equation

$$\mu_{gFPP} = \left(\frac{1}{C_{\mathrm{i}}}\right) \left(\frac{\delta\sigma}{\delta V_{\mathrm{GS}}}\right) \quad (3)$$

Figure 3b shows the V_{GS} dependence of the mobility employing the gFPP method. The mobility increases with V_{GS} and peaks at 15 $cm^2\ V^{-1}\ s^{-1}$ at $V_{GS} \approx$ -50 V, and then decreases with further increase in V_{GS}. The average of μ_{gFPP} over the entire V_{GS} range was ≈9.5 $cm^2\ V^{-1}\ s^{-1}$. This average μ_{gFPP} value is very close to effective mobility that was calculated using 100% reliability factor[25] in earlier section. The large decrease in mobility with increasing gate voltage suggests a large contact resistance in the two probe devices and becomes more prominent as the channel becomes less resistive at high gate voltage. The small decrease in the four-probe mobility (which eliminates contact resistance) at higher V_{GS}, is most likely due to traps and enhanced scattering of carriers resulting from their confinement to a progressively thinner channel at the semiconductor-dielectric interface.[27–29]

3.5 Organic Light-Emitting Transistors

Next, we fabricated LEFETs using heterostructures[17–18] comprised of aligned DPP-DTT polymer films as a charge transport layer and a solution processed polymer (Super Yellow, SY) or an evaporated small molecule (PCAN) as the light emitting layers. Their chemical structures can be seen in **Figure S3** (Supplementary Information). **Figure 4a** illustrates the LEFET structure comprising of a non-planar source drain electrode with Super Yellow. The charge carrier layers were again fabricated by dip-coating DPP-DTT films on

DTS treated nano-grooved substrates. **Figure 4c** shows the electrical characteristics for these LEFETs. Under negative voltage bias, they demonstrate linear and saturation regimes with current ON/OFF ratios of $>10^6$ and sharp turn-on voltages. The maximum effective hole mobility for the "hero" device was 7.6 $cm^2\ V^{-1}\ s^{-1}$ (calculated form a single linear slope of SQRT(I_{DS}) *versus* V_{GS} plot as shown in **Figure S5b** and at a 100% reliability factors, see **Table 2**). Sigmoidal output curves (at V_{DS} <8 V) in LEFETs (see **Figure S5**) indicate an extraction barrier for the holes.

Figures 4d and **4e** show the LEFET brightness and EQE as a function of gate voltage, respectively. Remarkably, the brightness increases with gate voltage, reaching a maximum of 29,000 cd m^{-2} at 0.4% EQE. For comparison, the EQE and brightness of samples without alignments[18a] were 0.04% at 900 cd m^{-2}. This brightness is the highest reported value in an LEFET to date [see **Tables 2 and S1**]. **Figure 4b** shows optical images of the devices. A bright yellow-green light in shape of the line adjacent to the electron-injecting electrode (Sm/Ba/Al) is visible with an emission zone width of 35 μm. These results clearly demonstrate the potential of nano-grooved substrate to simultaneously improve the brightness and mobility of LEFETs. We note that the Ba/Sm/Al electrode was not transparent and thus the measured light was only that which escaped around the edges of the electrode, leading to lower (EQE) than expected.

The used of nano-grooved substrates in LEFET structures has significant merit in achieving the high current densities required for electrically pumped lasing. However, calculating the actual current density is not straightforward. In a field effect transistor channel, the accumulation layer width is confined to a few nano-meters and results in high current density (> several kA cm^{-2}). This channel current density can lead to an overestimation of exciton current density values in LEFETs. Since the excitons in LEFETs are spread over the entire recombination zone width (35 μm), a significant lateral distribution area of the exciton density has to be considered. Therefore, from the width (35 μm) and the length of the light emission zone (2 mm), the maximum current density in the recombination zone at V_{GS} = -100 V is estimated to be 7 A cm^{-2}. This value is significantly higher than typical current density (mA cm^{-2}) in OLEDs. At high current density (>1 A cm^{-2}), the EQE roll-off indicates significant exciton quenching by the metal electrode (see **Figure S6**). We believe that by inserting an organic layer (for example an electron injecting material) between the luminescent layer and the metal electrode, electrode quenching could be completely eliminated.

We also fabricated a blue emitting LEFET using the above described technique to align DPP-DTT polymer films as a charge transport layer, but here in combination with the vacuum deposited small molecule emitter PCAN (**Figures 5a−f**) and an electron injecting layer of TPBI [1,3,5-tris(*N*-phenylbenzimidizol-2-yl)benzene] directly under the metal electrode. The PCAN-LEFETs give bright and narrow blue emission (**Figure 5b**) and their electrical transfer characteristics **(Figure 5c**) and output (**Fig S7)** reveal again a high hole current through the channel, caused by the aligned DPP-DTT polymer films underneath the emissive layer. PCAN based LEFETs also showed a high ON/OFF ratio (>10^5) and effective hole mobility 4.8 cm^2 V^{-1} s^{-1} (calculated form a single linear slope of SQRT(I_{DS}) *versus* V_{GS} plot as shown in **Figure S5b** and at a 100% reliability factor, see **Table 2**). The brightness also increased with gate voltage, reaching maximum brightness of 9,600 cd m^{-2} at 0.7% EQE. More importantly, the EQE does not roll-off at higher current density (9 A cm^{-2}) indicating elimination of exciton quenching near the metal electrode (see **Figure S8**). In contrast, the LEFET without TPBI layer showed significant EQE roll-off at 9 A cm^{-2}. We also note that the reported PCAN OLEDs[30] showed electrodes quenching at ≈100 mA cm^{-2}. The TPBI layer in LEFET structure indeed shifts the recombination zone away from the top drain electrode in a vertical direction (Z axis) and significantly reduces the exciton quenching by the drain electrode. However, at very high current densities, quenching due to polarons cannot be ruled out in LEFETs.

We note that the optical transparency of TPBI/Sm/Al was only ≈15% in the blue region thus reducing out-coupling efficiency and hence the EQE of these devices. The electro- and photoluminescence spectra of both the SY-LEFET and PCAN LEFET are shown in **Figure S9** in the Supplementary Information.

Figure S10 (Supplementary Information) shows the device-operating mechanism along with the materials' energy levels. Under negative gate bias (V_{GS} <0), holes are injected from the source electrode (Au) directly into the DPP-DTT layer, the latter having an ionisation potential (IP) of ≈5.1 eV.[24] With increasing gate voltage, holes are accumulated in the DPP-DTT film, which are the majority charge carriers in the LEFET channel. These holes move across the LEFET channel through the highly aligned DPP-DTT polymer. Seeking to reach the drain electrode under source-drain bias, they eventually pass into the light-emitting layer (SY or PCAN). Simultaneously, electrons are injected from the Ba/Sm (SY) or TPBI/Sm/Al (PCAN) electrode into the light-emitting layer resulting in exciton formation and subsequently light emission through electron injecting electrode (see transmission spectrum in Figure **S11)**.

This occurs at the vicinity of the electron-injecting electrode as shown in **Figures 4b, 5b** and **S10** (Supplementary Information).

4. Conclusions

In summary, we demonstrated a simple device fabrication strategy to obtain highly aligned polymer films applicable in both OFETs and LEFETs. The polymer films were prepared exploiting an inexpensive and simple substrate surface scratching technique prior to an economic dip-coating deposition. The resulting OFET devices exhibited "two slopes" in transfer characteristics. The origin of two shops were analysed and correlated with contact resistance and electron injection. Consequently, we fabricated hetero-structure LEFETs giving a record-breaking brightness of 29,000 cd m^{-2} at an EQE of 0.4% for yellow and 9,600 cd m^{-2} at 0.7% EQE for blue colours. Moreover, we achieved complete elimination of exciton quenching at current density up to 9 A cm^{-2} using an electron-injection buffer layer between the metallic electrode and light emitting layer. The high operating voltages in the reported LEFETs could be reduced by implementing a number of approaches including reducing the channel length, optimizing the channel with to length ratio and increasing the gate capacitance by employing high-k dielectrics or electrolyte gating.[31-33] These results are a significant advancement towards the ultimate goal of technologically viable solution processed LEFETs and pave the way to applications such as displays and electrically pumped organic lasers.

5. Experimental Methods

The substrates consisted of highly n-doped Si wafers with 200/400 nm thick of SiO_2/SiN_x deposited on top. These acted as the back-gate and dielectrics respectively. The substrates were cleaned by ultra-sonication in acetone and were structured with a diamond lapping sheet with 100 nm diamond particles. Substrates were cleaned again thoroughly by ultra-sonication in acetone and subsequently 2-propanol and dried before spin-coated with DTS (as described in **Figure S1**, Supplementary Information) from a solution of 0.5% in toluene. The Substrates were then annealed at 80 °C on a hot plate for 15 mins. DPP-DTT polymer solution was stirred on a hotplate (120 °C) for 2 hours and then kept at room temperature for at least 7 days to completely dissolve the polymer. The substrates were dipped into the polymer solution for 20 seconds and coating was completed by pulling the substrates at the rate of 0.2 mm per second by using a commercial dip-coater (Apex Xdip-SV1). Finally, these films were annealed at 200 °C on a hotplate for 1 hour in air.

For OFET devices, Au-Au symmetric electrodes were evaporated through shadow masks to form a channel width of 2 mm and channel length of 120 µm. Control OFETs were fabricated without structuring the substrates. OFETs were also fabricated with channels parallel and perpendicular to the polymer fibres on the same substrates to minimise the effects of process variation. The LEFET devices had asymmetric contacts, with Au as the source contact (thickness 35 nm) deposited directly on top of the DPP-DTT polymer layer using thermal evaporation through a shadow mask. For SY based LEFETs, the SY polymer was spin-coated on top of the DPP-DTT layer (with Au electrode) at 2,500 rpm for 30 seconds with a ramp up to 3000 rpm for 10 seconds. The devices were placed on a hotplate in a glove box and annealed at 150 °C for 30 minutes. Finally, the second electrode (as electron injection) comprised of sequential layers of Ba/Sm/Al, which was deposited by thermally evaporating these metals in high vacuum. For PCAN based LEFETs, the blue light emitting small molecule PCAN was thermally evaporated in high vacuum onto the DPP-DTT film and the Au electrode, followed by deposition of the electron injecting electrode, which was formed by evaporation of sequential layers of TPBI (≈40 nm), Sm (20 nm) and Al (20 nm) through a complementary shadow mask.

Characterisation of the devices were carried out using an Agilent B1500A Semiconductor Device Analyzer in conjunction with an SA-6 Semi-Auto Probe Station with a calibrated photomultiplier tube positioned above the devices. The brightness was measured directly by comparing the photocurrent in a PMT with a reference device of known brightness and light emission area. The photocurrent in the PMT was corrected for the effective light emitting area to get the correct brightness value. A Minolta Candela meter (LS-100) was used to measure the reference device brightness. The measurement of brightness and calculation of EQE were performed as standard procedure described earlier.[17–18] X-ray diffraction patterns were obtained with a PANalytical X'PERT PRO system using Cu Ka source (λ = 1.5418 Å) in air. The data were collected at still mode with 300 s per frame.

Acknowledgements

This work was funded by the Australian Research Council (DP140101088 and DP160100700) project. EBN is the recipient of The University of Queensland Fellowship. KM was funded by an Australian Postgraduate Award. This work was performed in part at the Queensland node of the Australian National Fabrication Facility Queensland Node (ANFF-Q)

– a company established under the National Collaborative Research Infrastructure Strategy to provide nano- and microfabrication facilities for Australia's researchers.

References

1. Hepp, A.; Heil, H.; Weise, W.; Ahles, M.; Schmechel, R.; von Seggern, H. Light-emitting field-effect transistor based on a tetracene thin film. *Phys. Rev. Lett.* **2003**, *91*, 157406.

2. Gwinner, M. C.; Kabra, D.; Roberts, M.; Brenner, T. J. K.; Wallikewitz, B. H.; McNeill, C. R.; Friend, R. H.; Sirringhaus, H. Highly efficient single-layer polymer ambipolar light-emitting field-effect transistors. *Adv. Mater.* **2012**, *24*, 2728–2734.

3. Zaumseil, J.; Friend, R. H.; Sirringhaus, H. Spatial control of the recombination zone in an ambipolar light-emitting organic transistor. *Nat. Mater.* **2006**, *5*, 69–74.

4. McCarthy, M. A.; Liu, B.; Donoghue, E. P.; Kravchenko, I.; Kim, D. Y.; So, F.; Rinzler, A. G. Low-voltage, low-power, organic light-emitting transistors for active matrix displays. *Science* **2011**, *332*, 570–573.

5. Roelofs, W. S. C.; Adriaans, W. H.; Janssen, R. A.; Kemerink, M.; Leeuw, D. M. Light emission in the unipolar regime of ambipolar organic field-effect transistors. *Adv. Funct. Mater.* **2013**, *23*, 4133–4139.

6. Capelli, R;. Toffani, S.; Generali, G.; Usta, H.; Facchetti, A.; Muccini, M. Organic light-emitting transistors with an efficiency that outperforms the equivalent light-emitting diodes. *Nat. Mater.* **2010**, *9*, 496–503.

7. Nakamura, K.; Hata, T.; Yoshizawa, A.; Obata, K.; Endo, H.; Kudo, K. Improvement of metal–insulator–semiconductor-type organic light-emitting transistors. *Jpn. J. Appl. Phys.* **2008**, *47*, 1889–1893.

8. Bisri, S. Z.; Takenobu, T.; Swabe, K.; Tsuda, S.; Yomogida, Y.; Yamao, T.; Hotta, S.; Adachi, C.; Iwasa, Y. p-i-n Homojunction in organic light-emitting transistors. *Adv. Mater.* **2011**, *23*, 2753–2758.

9. Ullah, M.; Armin, A.; Tandy, K.; Yambem, S. D.; Burn, P. L.; Meredith, P.; Namdas, E. B. Defining the light emitting area for displays in the unipolar regime of highly efficient light emitting transistors. *Sci. Reports* **2015**, *5*, 8818.

10. Muhieddine, K.; Ullah, M.; Pal, B. N.; Burn, P. L.; Namdas, E. B. All solution-processed, hybrid light emitting field-effect transistors. *Adv. Mater.* **2015**, *26*, 6410–6415.

11. Namdas, E. B.; Tong, M.; Ledochowitsch, P.; Mednick, S. R.; Yuen, J. D.; Moses, D.; Heeger, A. J. Low thresholds in polymer lasers on conductive substrates by distributed feedback nanoimprinting: progress toward electrically pumped plastic lasers. *Adv. Mater.* **2009**, *21*, 799–802.

12. Hsu, B. B. Y.; Duan, C.; Namdas, E. B.; Gutacker, A.; Yuen, J. D.; Huang, F.; Cao, Y.; Bazan, G. C.; Samuel, I. D. W.; Heeger, A. J. Control of efficiency, brightness, and

recombination zone in light-emitting field effect transistors. *Adv. Mater*. **2012**, *24*, 1171–1175.

13. Gwinner, M. C.; Khodabakhsh, S.; Song, M. H.; Schweizer, H.; Giessen, H.; Sirringhaus, H. Integration of a rib waveguide distributed feedback structure into a light-emitting polymer field-effect transistor. *Adv. Funct. Mater*. **2009**, *19*, 1360–1370.

14. Schols, S.; McClatchey, C.; Rolin, C.; Bode, D.; Genoe, J.; Heremans, P.; Facchetti, A. Organic light-emitting diodes with field-effect-assisted electron transport based on α,ω-diperfluorohexyl-quaterthiophene. *Adv. Funct. Mater.* **2008** *18*, 3645–3652.

15. Nakanotani, H.; Saito, M.; Nakamura, H.; Adachi, C. Highly balanced ambipolar mobilities with intense electroluminescence in field-effect transistors based on organic single crystal oligo(*p*-phenylenevinylene) derivatives. *Appl. Phys. Lett*. **2009**, *95*, 033308.

16. Takenobu, T.; Bisri, S. Z.; Takahashi, T.; Yahiro, M.; Adachi, C.; Iwasa, Y. High current density in light-emitting transistors of organic single crystals. *Phys. Rev. Lett*. **2008**, *100*, 066601.

17. a) Ullah, M.; Tandy, K.; Yambem, S. D.; Aljada, M.; Burn, P. L.; Meredith, P.; Namdas, E. B. Simultaneous enhancement of brightness, efficiency, and switching in RGB organic light emitting transistors. *Adv. Mater.* **2013**, *25*, 6213–6218; b) Ullah, M.; Wawrzinek, R.; Nagiri, R. C. R.; Lo, S.-C.; Namdas, E. B. UV–deep blue–visible light-emitting organic field effect transistors with high charge carrier mobilities. *Adv. Opt. Mater*. **2017**, DOI: 10.1002/adom.201600973.

18. a) Ullah, M.; Tandy, K.; Li, J.; Shi, Z.; Burn, P. L.; Meredith, P.; Namdas, E. B. High-mobility, heterostructure light-emitting transistors and complementary inverters. *ACS Photonics*, **2014**, *1*, 954–95; b) Ullah, M.; Tandy, K.; Clulow, A. J.; Burn, P. L.; Gentle, I. R.; Meredith, P.; Lo, S.-C.; Namdas, E. B. Host-free blue phosphorescent dendrimer organic light-emitting field-effect transistors and equivalent light-emitting diodes: A comparative study. *ACS Photonics*, **2017**, *4*, 754–760.

19. Hsu, Y.; B. B.; Seifter, J.; Takacs, C.; Zhong, C.; Tseng, H.-R.; Samuel, I. D. W.; Namdas, E. B.; Bazan, G. C.; Huang, F.; Cao, Y.; Heeger, A. J. Ordered polymer nanofibers enhance output brightness in bilayer light-emitting field-effect transistors. ACS *Nano* **2013**, *7*, 2344–2351.

20. Tseng, H.-R.; Phan, H.; Luo, C.; Wang, M.; Perez, L. A.; Patel, S. N.; Ying, L.; Kramer, E. J.; Nguyen, T.-Q.; Bazan, G. C.; Heeger, A. J. High-mobility field-effect transistors fabricated with macroscopic aligned semiconducting polymers. *Adv. Mater*. **2014**, *26*, 2993–2998.

21. Luo, C.; Kyaw, A. K. K.; Perez, L. A.; Patel, S.; Wang, M.; Grimm, B.; Bazan, G. C.; Kramer, E. J.; Heeger, A. J. General strategy for self-assembly of highly oriented

nanocrystalline semiconducting polymers with high mobility. *Nano Lett.* **2014**, *14*, 2764–2771.

22. Yuan, Y.; Giri, G.; Ayzner, A. L.; Zoombelt, A. P.; Mannsfeld, S. C. B.; Chen, J.; Nordlund, D.; Toney, M. F.; Huang, J.; Bao, Z. Ultra-high mobility transparent organic thin film transistors grown by an off-centre spin-coating method. *Nat. Commun.* **2014**, *5*, 3005.

23. Lee, B. H.; Bazan G. C.; Heeger, A. J. Doping-induced carrier density modulation in polymer field-effect transistors. *Adv. Mater.* **2016**, *28*, 57–62.

24. Li, J.; Zhao, Y.; Tan, H. S.; Guo, Y.; Di, C.-A.; Yu, G.; Liu, Y.; Lin, M.; Lim, S. H.; Zhou, Y.; Su, H.; Ong, B. S. A stable solution-processed polymer semiconductor with record high-mobility for printed transistors. *Sci. Reports* **2012**, *2*, 754.

25. Choi, H. H.; Cho, K; Frisbie, C. D.; Sirringhaus, H.; Podzorov V., Critical assessment of charge mobility extraction in FETs. *Nat. Mater.* **2018**, *17*, 2–7.

26. a) Bittle, E. G.; Basham, J. I.; Jackson, T. N.; Jurchescu, O. D.; Gundlach, D. J. Mobility overestimation due to gated contacts in organic field-effect transistors. *Nat. Comm.* **2016**, *7*, 10908; b) McCulloch, I.; Salleo, A.; Chabinyc, M. Organic devices. Avoid the kinks when measuring mobility. *Science.* **2016**, *352*, 1521–1522.

27. Uemura, T.; Rolin, C.; Ke, T. H.; Fesenko, P.; Genoe, J.; Hermans, P.; Takeya, J. On the extraction of charge carrier mobility in high-mobility organic transistors. *Adv. Mater.* **2015**, *28*, 151–155.

28. Phan, H.; Wang, M.; Bazan, G. C.; Nguyen, T. Q. Electrical instability induced by electron trapping in low-bandgap donor–acceptor polymer field-effect transistors. *Adv. Mater.* **2015**, *27*, 7004–7009.

29. Horowitz, G.; Hajlaoui, M. E.; Hajlaoui. R. Temperature and gate voltage dependence of hole mobility in polycrystalline oligothiophene thin film transistors. *J. Appl. Phys.* 2**000**. *87*, 4456.

30. Cho, I.; Kim, S. H.; Kim, J. H.; Park, S.; Park, S. Y. Highly efficient and stable deep-blue emitting anthracene-derived molecular glass for versatile types of non-doped OLED applications. *J. Mater. Chem.* **2012**, *22*, 123–129.

31. Schwabegger, G.; Ullah, M.; Irimia-Vladu, M.; Baumgartner, M.; Kanbur, Y.; Ahmed, R.; Stadler, P.; Bauer, S.; Sariciftci, N. S.; Sitter, H. High mobility, low voltage operating C60 based n-type organic field effect transistors. *Synth. Met.* **2011**, *161*, 19−20, 2058−2062.

32. Ullah, M.; Wawrzinek, R.; Maasoumi, F.; Lo, S.-C.; Namdas, E. B. Semitransparent and low-voltage operating organic light-emitting field-effect transistors processed at low temperatures. *Adv. Opt. Mater*. **2016**, *4*, 1022–1026.

33. Cho, J. H.; Lee, J.; Xia, Y.; Kim, B. S.; He, Y.; Renn, M. J.; Lodge, T. P.; Frisbie, C. D. Printable ion-gel gate dielectrics for low-voltage polymer thin-film transistors on plastic. *Nat. Mater*. **2008**, *7*, 900−908.

Table 1: A summary of the OFET mobilities and reliability factors.

Devices	$\mu_{lower\ slope}$ **($cm^2\ V^{-1}\ s^{-1}$)**		$\mu_{higher\ slope}$ **($cm^2\ V^{-1}\ s^{-1}$)**		μ_{eff} **($cm^2\ V^{-1}\ s^{-1}$)**
	$\mu_{calculated}$	r (%)	$\mu_{calculated}$	r (%)	
Aligned -Parallel	5	188	13	72	9.4
Control	2	88	0.8	202	1.6
Aligned - Perpendicular	0.88	102	0.88	102	0.9

Table 2: A summary of the optoelectronic properties of the devices used for this study. Averages were taken for at least 5 devices. Errors given are the standard deviation of the results

	Super Yellow	**PCAN**
μ_{eff} **(cm^2 V^{-1} s^{-1})** **(*r* = 100%)**	7.6	4.8
ON/OFF	$>10^6$	$>10^5$
Brightness (cd m^{-2})	29,000±2,000	9,600±600
EQE (%)	0.4±0.1	0.7±0.1

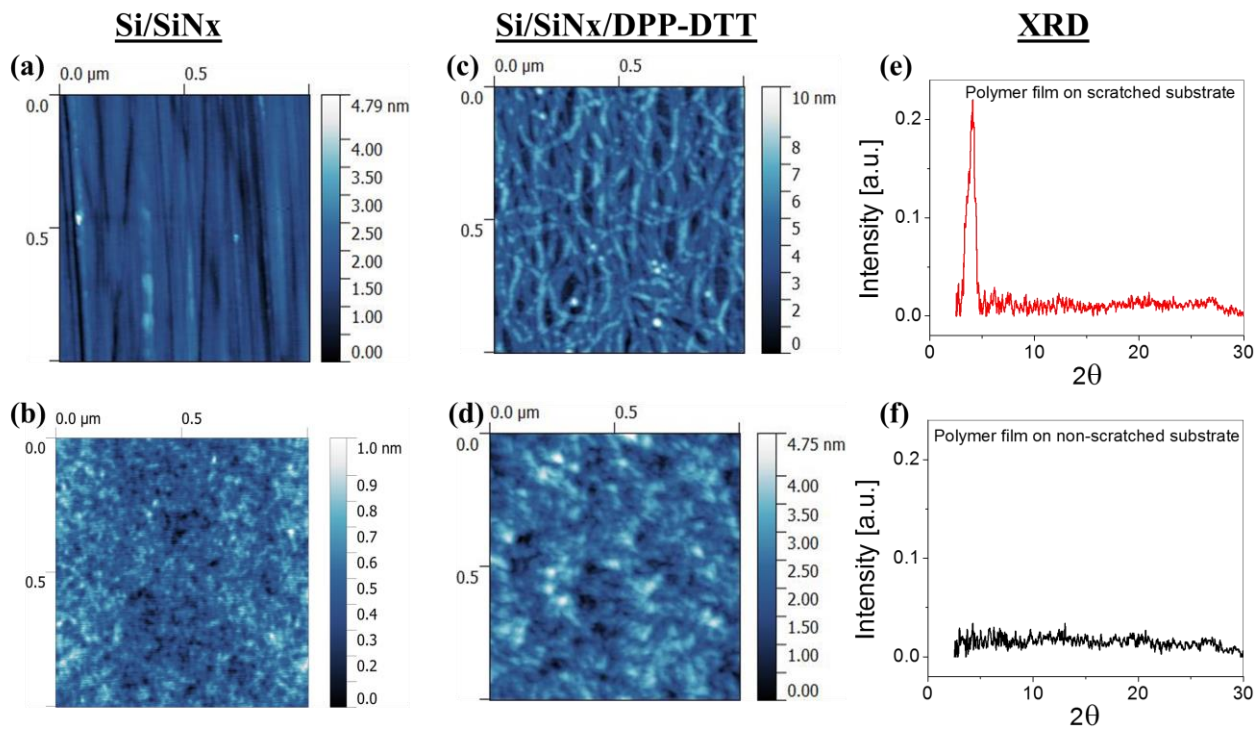

Figure 1: AFM topographic images of (a) scratched SiNx surface (b) unscratched (control) SiNx, (c) polymer film on scratched substrate and (d) polymer film on unscratched substrate. XRD graphs of polymer film on scratched substrate (e) polymer film on unscratched (control) substrate (f).

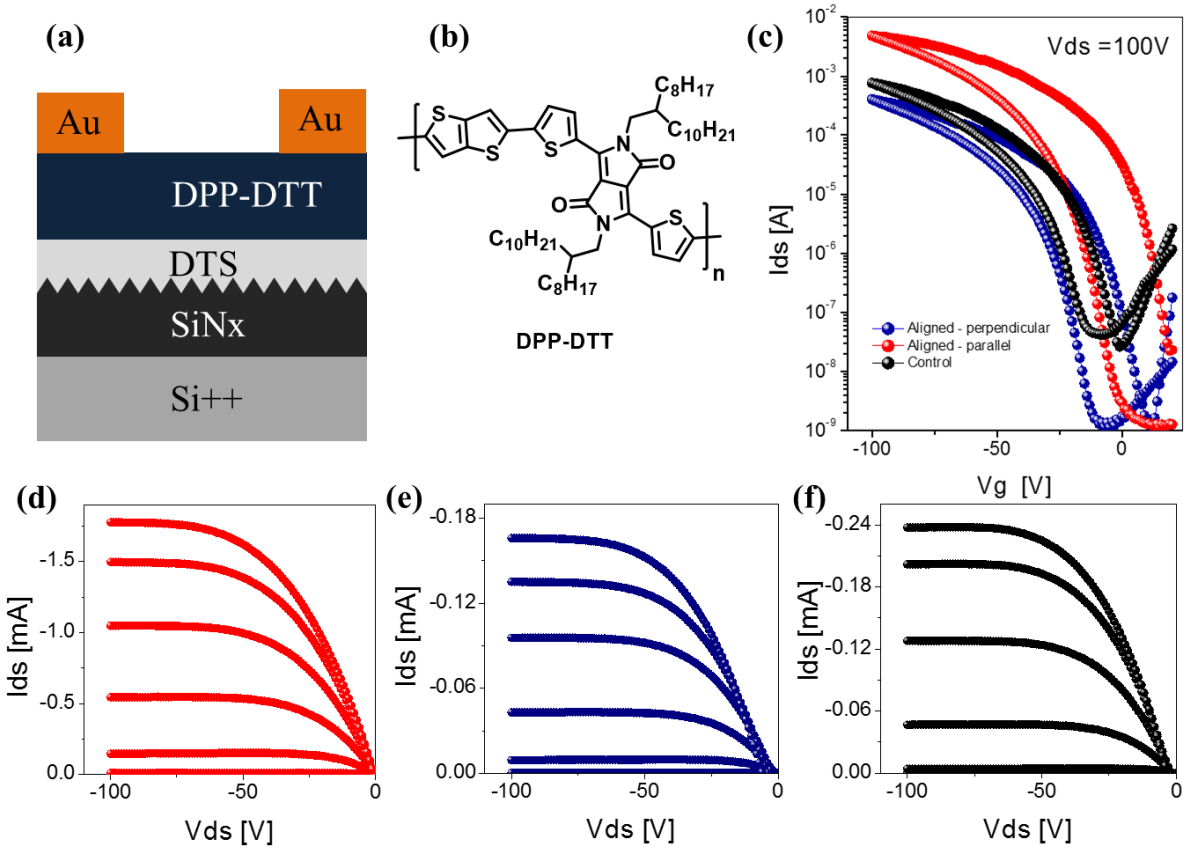

Figure 2: OFETs: (a) Device structure, b) molecular structure of DPP-DTT. (c) Transfer characteristics of three OFETs. d) Output characteristics of the aligned polymer along parallel direction to the transistor channel, (e) perpendicular to the scratched and (f) without scratches (control).

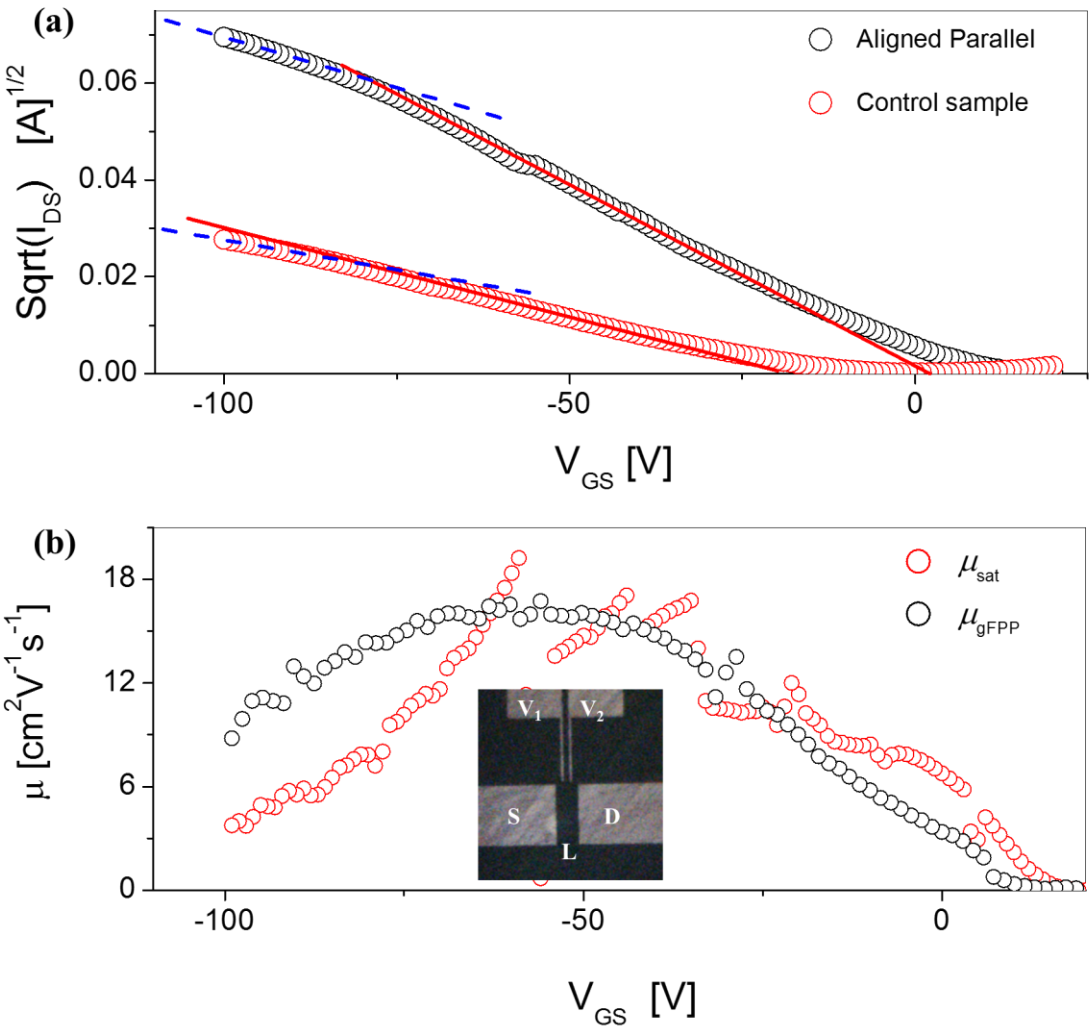

Figure 3: (**a**) Square root of source drain current for control and nano-grooved OFETs with channel length L = 120 µm, and channel width= 2,000 µm. (**b**) V_{GS} dependent OFET mobility measured in saturation regime (V_{DS} = -100 V; for L = 120 µm, W = 2,000 µm) and gFPP method (V_{DS} = -10 V). Inset shows the gFPP geometry with channel length with channel length L = 500 µm, and channel width = 1,000 µm, source electrode S, drain electrode D, and voltage probes V_1 and V_2.

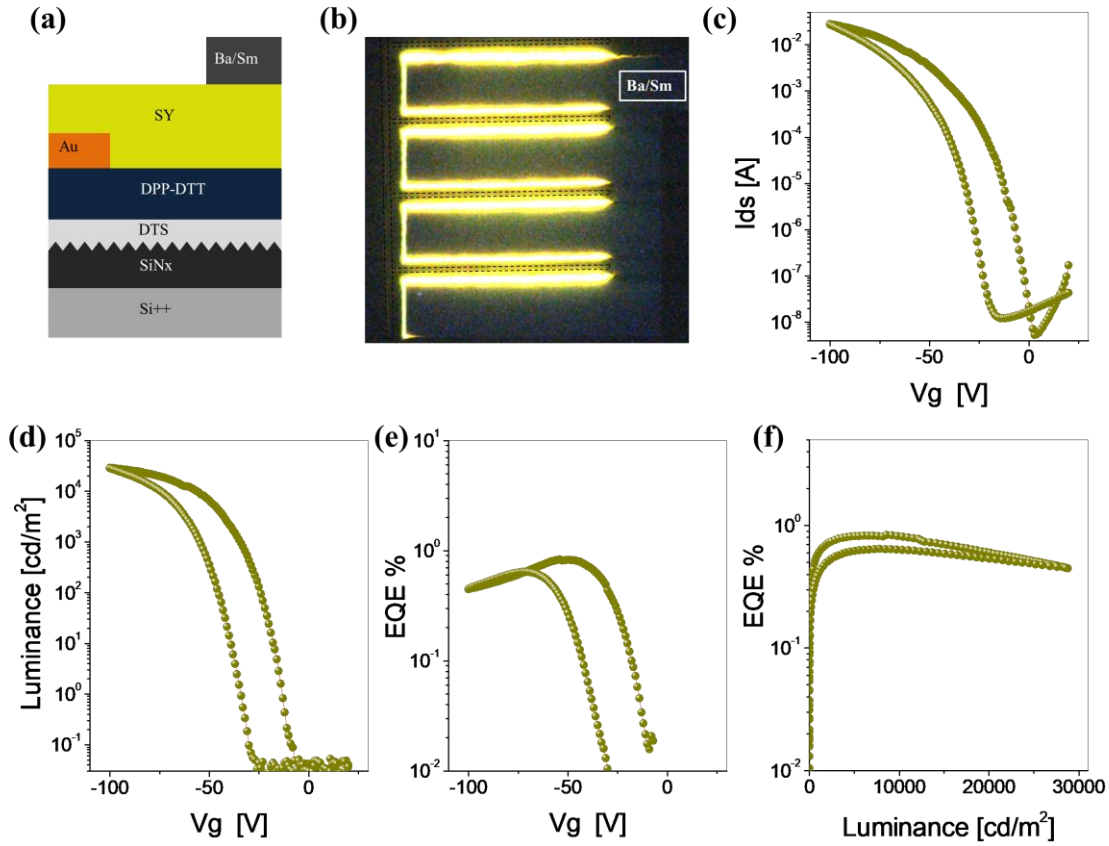

Figure 4: Super Yellow based LEFETs: (a) The LEFET device structure used in this study, (b) micrograph of light emission of the device, (c) the transfer characteristic of the LEFET. Optical characteristics in terms of (d) Luminance *versus* gate voltage, (e) EQE *versus* gate voltage and EQE *versus* Luminance (f)

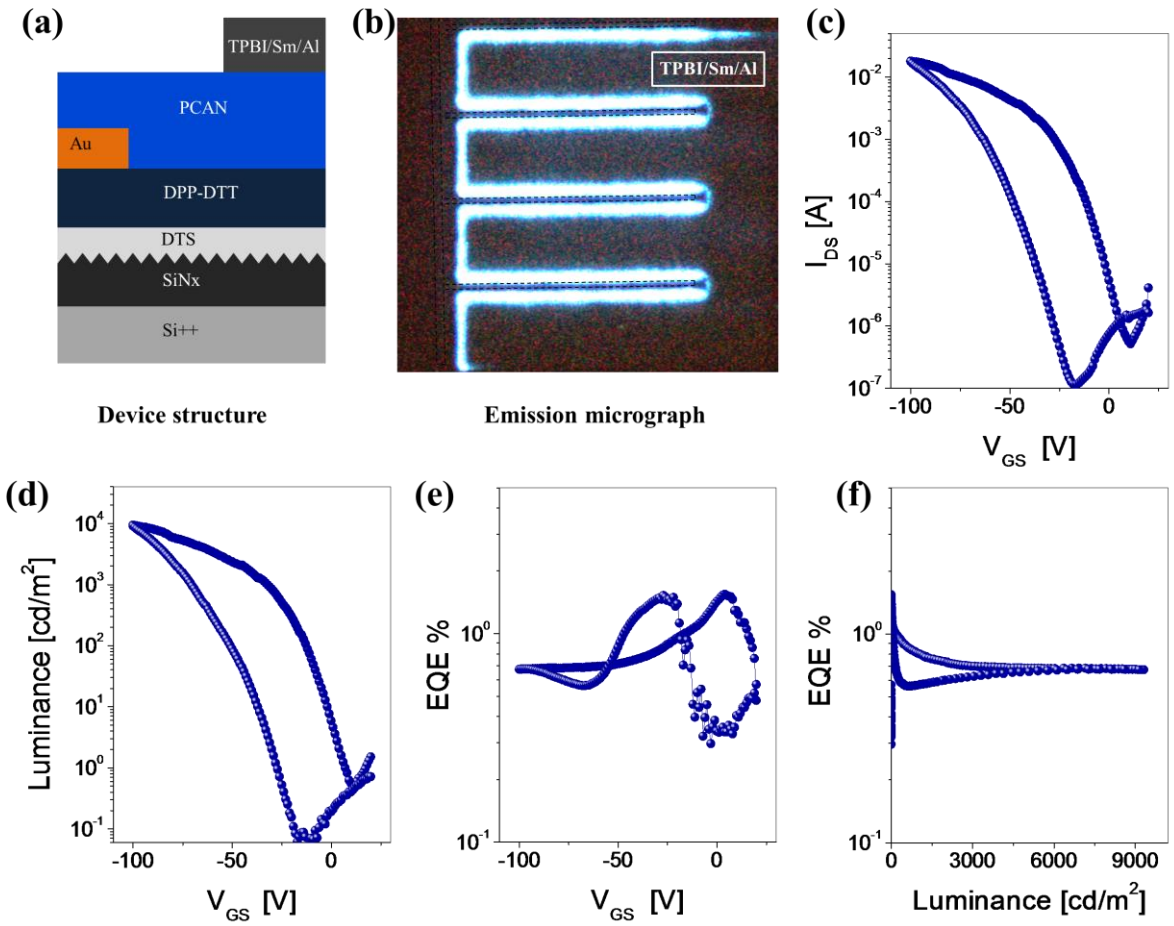

Figure 5: PCAN based LEFETs: (a) The LEFET structure used in this study, (b) micrograph of light emission of the device, (c) the transfer characteristic of the LEFET. Optical characteristics in terms of (d) Luminance *versus* gate voltage, (e) EQE *versus* gate voltage and EQE *versus* Luminance (f)